Insight from first principles into the nature of the bonding between water molecules and 4*d* metal surfaces

Javier Carrasco,[1,2] Angelos Michaelides,[1,2,a)] and Matthias Scheffler[1]
[1]*Fritz-Haber-Institut der Max-Planck-Gesellschaft, Faradayweg 4-6, D-14195 Berlin, Germany*
[2]*Department of Chemistry, London Centre for Nanotechnology, University College London, London WC1E 6BT, United Kingdom*

(Received 25 January 2009; accepted 3 April 2009; published online 11 May 2009)

We address the nature of the bond between water molecules and metal surfaces through a systematic density-functional theory (DFT) study of H_2O monomer adsorption on a series of close-packed transition metal surfaces: Ru(0001), Rh(111), Pd(111), and Ag(111). Aiming to understand the origin behind energetic and structural trends along the 4*d* series we employ a range of analysis tools such as the electron reactivity function, decomposition of densities of states, electron density differences, and inspection of individual Kohn–Sham orbitals. The results obtained from our DFT calculations allow us to rationalize the bonding between water and transition metal surfaces as a balance of covalent and electrostatic interactions. A frontier orbital scheme based on so-called two-center four-electron interactions between the molecular orbitals of H_2O—mainly the $1b_1$— and *d*-band states of the surface proves incisive in understanding these systems. © *2009 American Institute of Physics*. [DOI: 10.1063/1.3125002]

I. INTRODUCTION

H_2O-solid interactions play a prominent role in many aspects of scientific endeavor. In particular, the interaction of water with metals is central to fields such as materials science, corrosion, catalysis, and electrochemistry.[1–4] Key to understanding the role water plays in these disciplines is an attainment of fundamental atomic- and electronic-level understanding of the nature of the bond between water molecules and metal surfaces. This is what we target in the current paper, which reports a systematic theoretical study, with a predictive first principles approach, of the adsorption of individual water monomers on a number of close-packed 4*d* metal surfaces. Although van der Waals interactions will play a role in the bonding of water monomers to metal surfaces, it is usually assumed that the bonding stems mainly from a combination of orbital and electrostatic interactions.[5,6] Since the water molecular dipole is pretty large, 1.8 D in the gas phase, one could foresee a significant role of the molecular dipole with the substrate through a metal image dipole interaction.[7–9] However, a simple electrostatic picture which such a model apparently implies does not agree with the parallel-like water adsorption geometry claimed to occur for water monomers on many close-packed metal surfaces.[6,10–21] Instead this configuration has been rationalized in terms of covalent bonding interactions between *d* states of the substrate and specific molecular orbitals of the adsorbate.[5,6,18,22,23] In particular, the role of the water $1b_1$ lone pair orbital in the bonding appears to be crucial.

Notwithstanding the general insight and the tremendous amount of work performed on these seemingly simple adsorption systems[5,6,10–25] the precise details of the nature of the bond between water monomers and close-packed metal surfaces remains a matter of debate.[25–30] Important questions remain unanswered, such as, for example: (i) What is the role of partial and full occupation of the *d*-band when moving along the transition metal series? and (ii) What precisely is the role of the $1b_1$ lone pair orbital and how does it steer the water adsorption geometry? Indeed there are currently two different flavors to describe the role the $1b_1$ orbital plays in these adsorption systems: One which is based upon a covalent bonding mechanism and another that is based on charge redistribution in order to reduce Pauli repulsion with the substrate.[25,31] Can these two pictures be merged in some way? The main aim of the present work is to tackle these and related issues by understanding in detail the nature of the electronic structure that lies behind these adsorption systems and in so-doing build an overall bonding model for monomeric water on close-packed metal surfaces. To this end, we present results from density-functional theory (DFT) concerning the study of the adsorption of water monomers on a series of close-packed 4*d* metal surfaces: Ru(0001), Rh(111), Pd(111), and Ag(111). The many interesting properties of adsorbed water clusters and extended two-dimensional (2D) water overlayers, which have received much attention in recent years, are out of the scope of the present work.

The rest of this paper is organized as follows. The computational details and theoretical methods used to analyze our results are described in Sec. II. Section III begins with a brief discussion of the electronic reactivity of the clean metal surfaces and the gas phase water molecule. Water adsorption energies and geometries are discussed in Sec. III B. The interaction between the water dipole moment and its image inside the surface is then considered from a pure electrostatic point of view in Sec. III C. Analysis of electron densities and density of states in these adsorption systems is presented in Secs. III D and III E, respectively. Further analysis and the

[a)]Electronic mail: angelos.michaelides@ucl.ac.uk.

construction of interaction diagrams based on frontier orbital arguments are given in Sec. III F. Finally, we close in Sec. IV with a discussion and conclusions.

II. METHODOLOGY AND COMPUTATIONAL DETAILS

Adsorption energies and geometries have been obtained through a series of DFT calculations within a periodic slab approach using the CASTEP code.[32] Preliminary calculations including the usual tests of supercell size, vacuum spacing between slabs, plane wave cutoff, and number of **k**-points for the first Brillouin zone sampling, were first performed to establish a consistent and reliable numerical setup. Vanderbilt ultrasoft pseudopotentials[33] were used throughout, expanded within a plane wave basis set with a cutoff energy of 400 eV. The Perdew–Burke–Ernzerhof[34] (PBE) exchange-correlation functional was used together with a Monkhorst–Pack[35] grid with at least $12\times12\times1$ **k**-point sampling per 1×1 cell. Most geometry optimizations were started from the orientations obtained previously[5] and reoptimized with the current setup with a convergence threshold of 0.01 eV/Å on the atomic forces. Water was adsorbed within a $p(2\times2)$ unit cell cut along the (111) direction for Rh, Pd, and Ag, and along the (0001) plane for Ru, containing in all cases four atomic layers separated by 14 Å of vacuum. The atoms in the bottom layer were fixed at their bulk-truncated PBE positions.[36]

We have employed standard analysis tools to reach an understanding of the fundamental interactions involved in water-metal bonding. Specifically we have explored the behavior of the projected density of states (PDOS), electron density difference ($\Delta\rho$), and the electron density of the Kohn–Sham eigenstates.[37] Here $\Delta\rho$ is defined as

$$\Delta\rho = \rho[\mathrm{H_2O}/M] - \rho[\mathrm{H_2O}] - \rho[M], \tag{1}$$

where $\rho[\mathrm{H_2O}/M]$, $\rho[\mathrm{H_2O}]$, and $\rho[M]$ are the electron densities of the interacting system (H_2O plus the metal slab), an isolated H_2O molecule and the clean metal slabs, respectively. We have also employed the so-called electronic reactivity function or Wilke function, $W(\mathbf{r})$, based on the concepts developed by Fukui and co-workers[38,39] and Wilke *et al.*:[40]

$$W(\mathbf{r}) = \frac{1}{k_B^2 T_{\mathrm{el}}}\left(\frac{\partial\rho(\mathbf{r},T_{\mathrm{el}})}{\partial T_{\mathrm{el}}}\right) \approx \frac{\rho(\mathbf{r},T_{\mathrm{el},2}) - \rho(\mathbf{r},T_{\mathrm{el},1})}{k_B^2 T_{\mathrm{el},2}(T_{\mathrm{el},2} - T_{\mathrm{el},1})}, \tag{2}$$

where k_B is the Boltzmann constant and $k_B T_{\mathrm{el}}$ stands for the broadening parameter, where T_{el} is the artificial electronic temperature. $W(\mathbf{r})$ is especially useful for treating systems that show weak interactions such as water adsorption on metals. Through $W(\mathbf{r})$ it is possible to characterize the local reactivity of a metal surface before adsorption. The Wilke function derives from the hard and soft acid and base principle introduced by Pearson and co-workers.[41–43] Soft species can change their electronic configuration easily, i.e., the valence electrons can be polarized, removed or added with a low energy cost. On the other hand, hard species show the opposite behavior. When two reactants interact, either hard-hard or soft-soft interactions are preferred. Wilke *et al.* proposed a convenient measure of the spatial distribution of $W(\mathbf{r})$ for metal surfaces, which characterizes the local polarizability of the surface. It is based on the changes in the electronic states close to the Fermi level, E_F, due to the broadening of the occupation numbers in this frontier region. Positive (negative) regions in $W(\mathbf{r})$ plots indicate electron states that can be easily occupied (depleted). In practice, we have computed $W(\mathbf{r})$ from two different electron densities, $\rho(\mathbf{r},T_{\mathrm{el},1})$ and $\rho(\mathbf{r},T_{\mathrm{el},2})$, calculated with different broadening parameters, $k_B T_{\mathrm{el},1}=1.4$ meV and $k_B T_{\mathrm{el},2}=123.8$ meV. These two self-consistent calculations were performed at the optimized relaxed geometries, employing a $p(1\times1)$ unit cell and a 6 layer slab. Since $W(\mathbf{r})$ is extremely sensitive to the first Brillouin zone (IBZ) sampling, highly dense **k**-point meshes are mandatory in order to obtain converged plots.[44] Here 938 **k**-points in the IBZ ($25\times25\times3$) have been employed in order to obtain the plots of $W(\mathbf{r})$.

III. RESULTS

A. Electronic reactivity function of the isolated fragments: Substrate and water

Prior to water adsorption, we consider the local isoelectronic reactivity function, $W(\mathbf{r})$, of the clean Ru(0001), Rh(111), Pd(111), and Ag(111) surfaces, and then the isolated gas phase water molecule. From Fig. 1 it is clear that at all considered metal surfaces a pronounced inhomogeneity in $W(\mathbf{r})$ is observed, with distinct regions of "softness" at all distances from the surfaces displayed. The magnitude of the population and depletion regions is not the same for all metals. In particular, the largest changes are observed for Pd(111) and the smallest for Ag(111). Further, it can be noticed that the features of $W(\mathbf{r})$ differ substantially when moving along the *d*-metal series. Specifically, the clover-shaped regions common to the Ru, Rh, and Pd[45] surfaces switch in sign upon moving from Ru to Pd. This simply reflects that the nature of the orbitals involved in each case is different, which, obviously, reflects the different occupation of the *d* states. When considering the interaction of water with these surfaces, soft zones (either dark red or dark blue in Fig. 1) are particularly interesting as potential sites for water adsorption. The specific topology of such regions depends on the considered height above the surface and the metal. As will be shown in Sec. III B, after adsorption the water-metal distances are in the range of 2.3–2.7 Å and, therefore, it is reasonable to expect that the reactivity of the surface will be determined by the topology of $W(\mathbf{r})$ at distances above ≈1 Å (roughly half of the water-metal distance). At distances around $Z=1.0-1.5$ Å soft regions are centered essentially around atop sites (dark blue and dark red zones in Fig. 1) in all cases, pointing out that such sites (as we know) are likely targets for water adsorption.

Let us move now to briefly discuss the electronic structure of an isolated H_2O molecule. The core region is comprised of $1a_1$ and $2a_1$ states, essentially oxygen $1s$ and $2s$. Outside this in the valence region there are, in order of increasing energy, the $1b_2$, $3a_1$, and $1b_1$ states. The $3a_1$ and $1b_1$ states are the highest energy valence states of water, and thus are the most likely to be involved in bonding. The highest occupied molecular orbital, the nonbonding $1b_1$, is

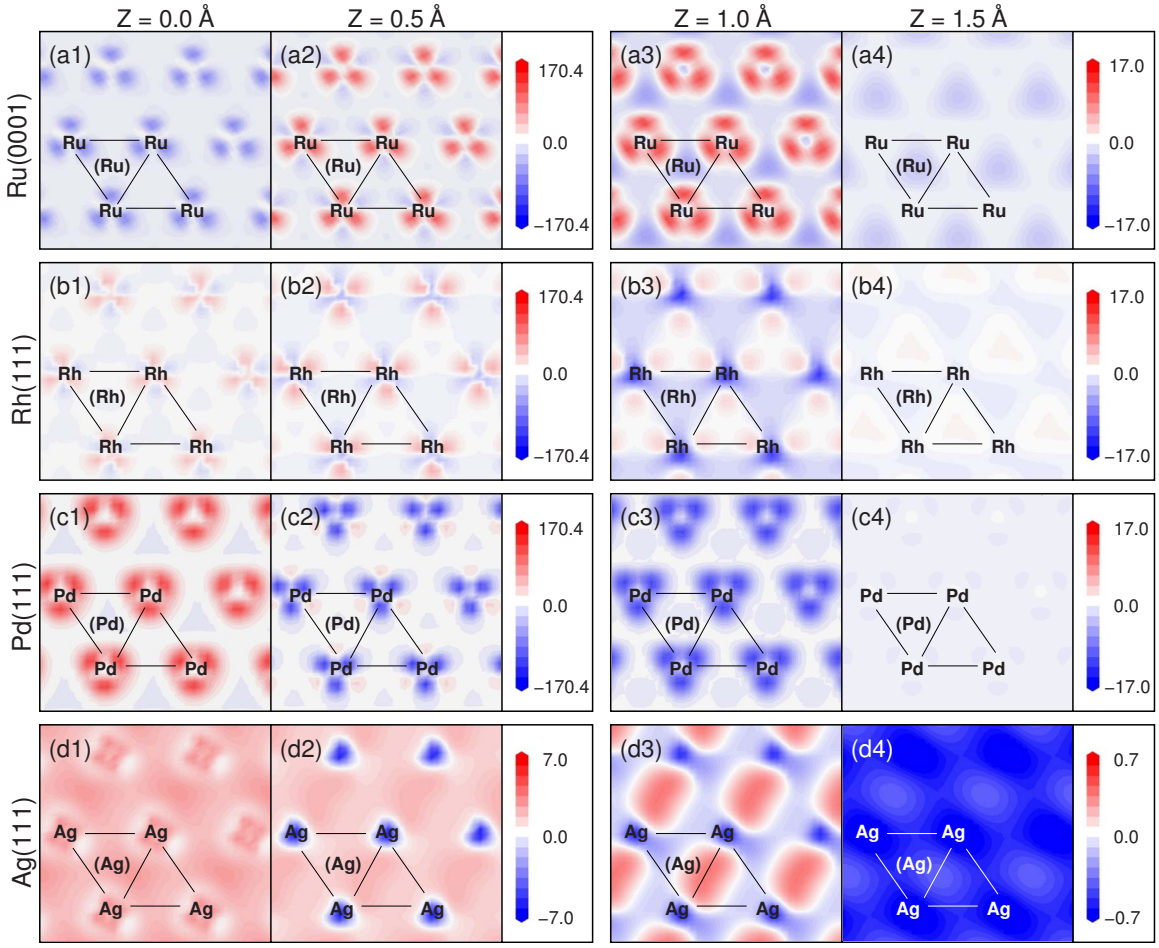

FIG. 1. (Color online) Plots of the function $W(\mathbf{r})$ for clean metal surfaces: (a) Ru(0001), (b) Rh(111), (c) Pd(111), and (d) Ag(111) along planes parallel to each surface at four different heights $Z=0.0$ Å, $Z=0.5$ Å, $Z=1.0$ Å, and $Z=1.5$ Å. Red regions can accept additional electrons, while blue ones can readily donate electrons. The position of the metal atoms on the surface and in the subsurface are indicated. The units are 10^{-2} Å^{-3} eV^{-2}. Note that $W(\mathbf{r})$ for the Ag surface is displayed on a different scale.

mainly an oxygen p-like lone pair perpendicular to the molecular plane. The $3a_1$ orbital sits about 2.0 eV below the $1b_1$ and is comprised primarily of O p character residing in the plane of the molecule plus some weak H s contribution.

In Figs. 2(a) and 2(b) the free water molecule is analyzed in terms of the reactivity index, $W(\mathbf{r})$. A clear electron depletion region is observed around the periphery of the water molecule corresponding to the spatial domains associated with the occupied $3a_1$ and $1b_1$ orbitals, while the region around the oxygen atom shows potential for electron accumulation associated with the first unoccupied state, the $4a_1$ orbital. We will see below that the electron rearrangement within the water molecule upon adsorption largely resembles these plots of $W(\mathbf{r})$. Water, when approaching parallel to the surface, is then electronically soft and, therefore, it interacts efficiently with soft surface regions, i.e., atop sites and their vicinity as pointed out previously and as discussed in more detail in Sec. III B.

B. Adsorption energies and geometries

As pointed out in previous DFT studies,[5,18,21] on all the metals considered here water monomers adsorb on atop sites and lie almost parallel to the surface. By almost parallel we mean that the tilt angle (α) between the molecular plane and the surface ranges from 0.5° to 11.5° (Table I and Fig. 2). In addition, the angle δ between the surface normal and the oxygen atom of the water molecule shows small values ranging from 3.0° to 7.6° across the different metal surfaces. And the azimuthal angle, ϕ, exhibits a slight energetic preference for the O–H bonds to be directed toward the nearest adjacent metal atoms on the surface. Overall the potential energy surface of water adsorption on these surfaces is quite flat in the vicinity of the atop site and rather insensitive to small changes of a few degrees in α, δ, and ϕ. In a range of $\pm 5°$ for α and δ around the minimum, the total energy change is less than 5 meV (Fig. 3). Besides, the rotation of the water molecules with the O atom pinned to the atop metal site (ϕ) shows also a flat dependence [Fig. 3(c)]. On each surface the internal H–O–H angle (θ) of the water molecule is expanded very slightly by $\leq 1°$ with respect to the gas phase geometry. The metal-oxygen distance (d_{M-O}) is about 2.3 Å for Ru, Rh, and Pd and about 2.7 Å for Ag. As can be seen from Table I, the computed adsorption energies[46] decrease in the sequence Ru > Rh > Pd > Ag, ranging from −0.42 to −0.15 eV. All these results are largely consistent with previous work on these adsorption systems.[5,18]

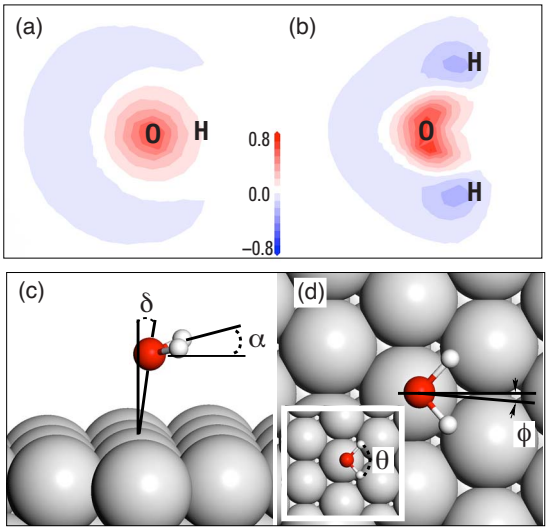

FIG. 2. (Color online) Side (a) and top (b) 2D contour plots of the function $W(\mathbf{r})$ for a free H_2O molecule in gas phase. The units are 10^{-2} Å^{-3} eV^{-2}. Side (c) and top (d) view of a H_2O monomer adsorbed on a close-packed metal surface. Notice that the angle α describes the tilt angle formed by the water molecular plane and the metal surface, while δ is defined as the angle between the surface normal and a vector between oxygen and the atop metal atom.

C. Metal image dipole interaction

In trying to understand these adsorption systems we first consider the role electrostatics play, focusing, in particular, on the importance of the permanent water dipole moment of the water molecule. Indeed the electrostatic dipole interaction with the substrate through a metal image dipole is attractive in nature and, with few exceptions,[47] said to favor a perpendicular water adsorption configuration.[5,7,8] We have considered here explicitly a classical model developed by Maschhoff and Cowin[8] to quantify the interaction between an adsorbed dipole and the image-charge induced on the metal surface. From a pure classical model an adsorbed molecule is assumed here to have an unperturbed dipole moment $\mu_0 = q \cdot d$ and the dipole can be modeled then by two point charges $\pm q$ with a d molecular dipole length [Fig. 4(a)]. The energy of the dipole in its self-induced field—without considering its internal polarization—located β away from the metal image plane is given by[8]

$$U_{se} = \frac{q^2}{8\pi\epsilon_0} G(\beta, d), \tag{3}$$

where $G(\beta,d)$ is a factor which depends on the adsorbed dipole geometry, i.e., β and d. We have considered here two different dipole orientations to the surface: Vertical and flat.

TABLE I. Adsorption energies, E_{ads}, interatomic distances, and tilt angles of adsorbed H_2O on metal surfaces.

	E_{ads} (eV)	d_{M-O} (Å)	d_{O-H} (Å)	θ (deg)	α (deg)	δ (deg)
Ru(0001)	−0.42	2.31	0.99	105.3	11.5	3.0
Rh(111)	−0.36	2.34	0.99	104.6	4.2	4.1
Pd(111)	−0.27	2.33	0.98	104.8	5.1	5.4
Ag(111)	−0.15	2.67	0.98	104.2	0.5	7.6

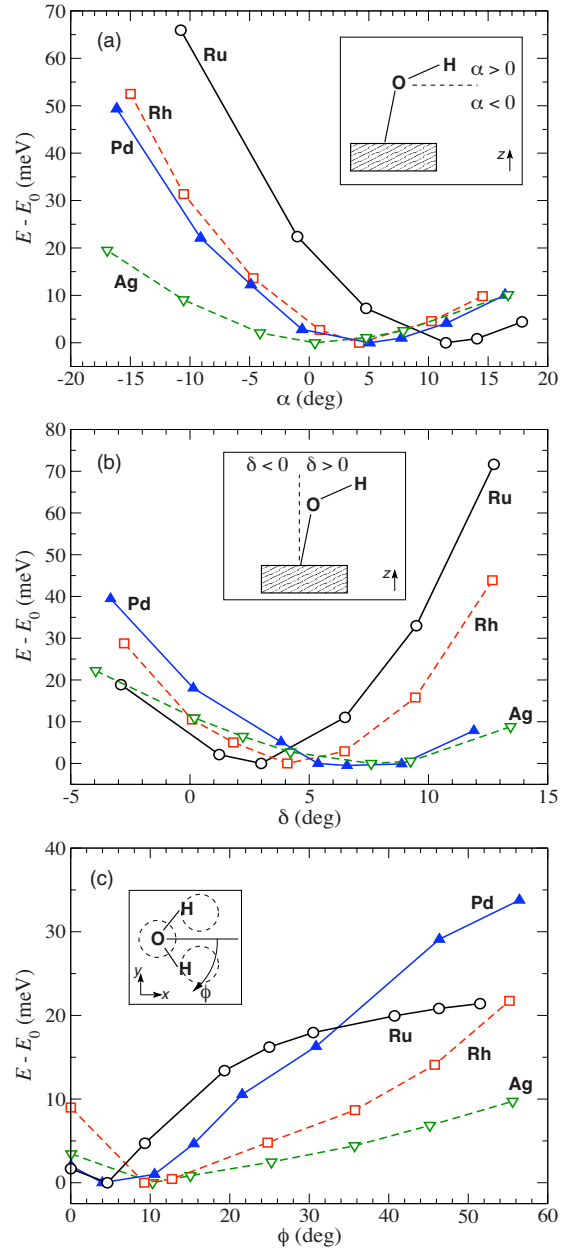

FIG. 3. (Color online) Relative energy against (a) α, (b) δ, and (c) ϕ angles. See Fig. 2 for definitions of α, δ, and ϕ. $\alpha=0°$ corresponds to H_2O parallel to the surface; negative α indicates water orientations with the H atoms pointing toward the surface. $\delta=0°$ corresponds to O sitting exactly at an on-top site. At $\phi=0°$ the dipole vector of the water molecule is directed toward an adjacent bridge site of the substrate.

For each case the explicit expression for $G(\beta,d)$ becomes

$$G^{\text{vertical}} = -\frac{1}{2\beta + d} - \frac{1}{2\beta - d} + \frac{1}{\beta}, \tag{4}$$

and

$$G^{\text{flat}} = -\frac{1}{\beta - d/2} + \frac{2}{\sqrt{d^2 + 4(\beta - d/2)^2}}, \tag{5}$$

for vertical and flat orientations, respectively.

In order to compare the relative stability of vertical and flat orientations for a given adsorbed dipole geometry, we have computed the difference between U_{se}^{vertical} and U_{se}^{flat}. U_{se} is always negative, since it represents a charge-to-image-

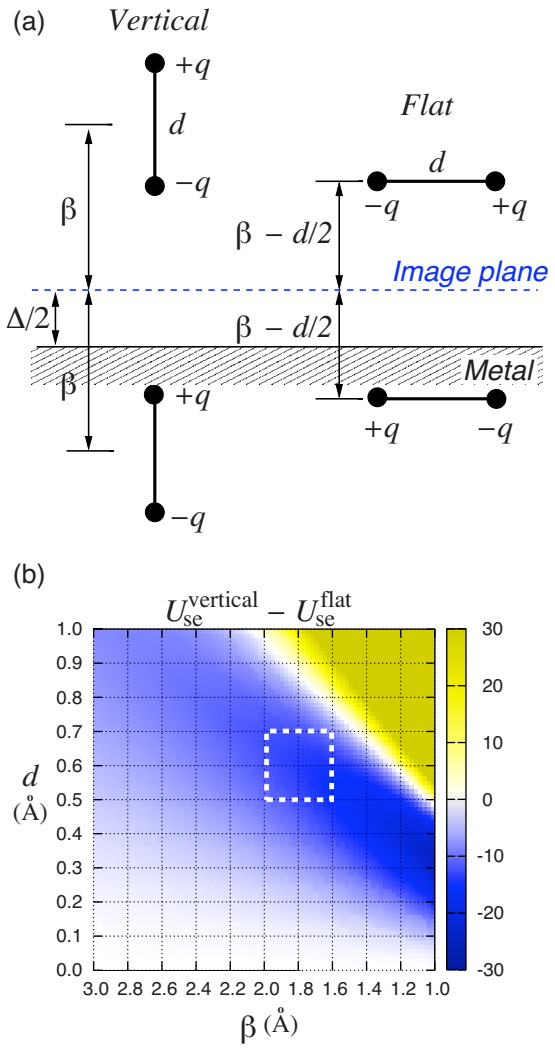

FIG. 4. (Color online) (a) Schematic of the electrostatic interaction model between a metal surface and an adsorbed dipole at vertical and flat orientations (see text for a description of the different parameters). (b) The calculated difference values between U_{se} terms for vertical and flat orientations: $U_{se}^{vertical} - U_{se}^{flat}$ (in meV). A dipole charge equal to $\pm 0.80e$ has been considered. The dashed rectangle indicates the most probable physical region.

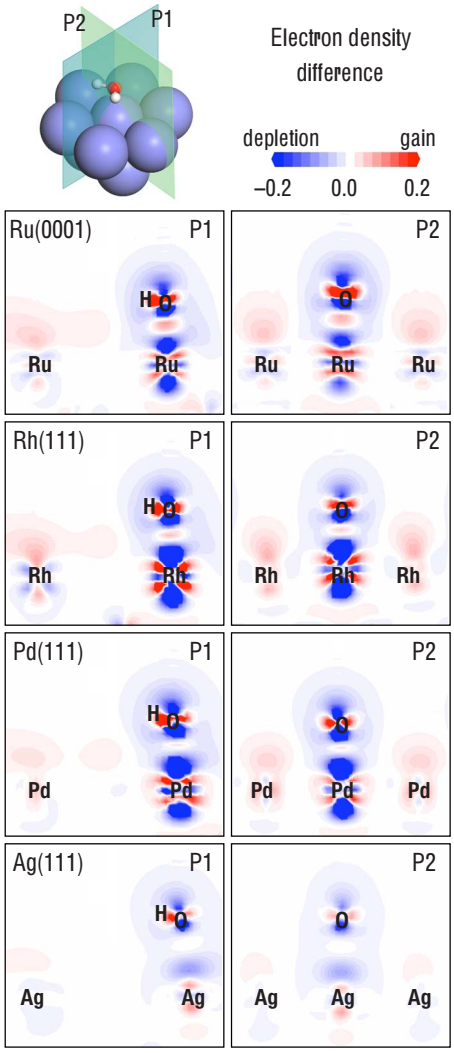

FIG. 5. (Color online) 2D slices of $\Delta\rho$ for monomeric H_2O adsorbed on Ru(0001), Rh(111), Pd(111), and Ag(111). The cartoon at the top depicts the two different planes along which $\Delta\rho$ slices have been made. Notice that while plane P1 is precisely perpendicular to the metal surface, plane P2 is slightly tilted by δ degrees (see Table I and Fig. 2), containing both the oxygen of water and the substrate metal atom to which it is directly linked. $\Delta\rho$ is in units of eÅ^{-3}.

charge attraction. Therefore, $(U_{se}^{vertical} - U_{se}^{flat}) < 0$ indicates that the vertical orientation is favored over the flat one. Figure 4(b) shows $(U_{se}^{vertical} - U_{se}^{flat})$ for a range of β(1.0–3.0 Å) and d(0.0–1.0 Å) parameters and setting an arbitrary dipole charge of $\pm 0.80e$—the Mulliken charge of the oxygen atom when water is adsorbed on the different metal surfaces ranges from $-0.76e$ (on Ru) to $-0.86e$ (on Ag).[48] Two clear preferred orientation domains can be distinguished depending on the considered β-d set. The region where a vertical orientation is favored corresponds to the most probable physical situation. Specifically, for a water molecule a realistic value for d should be around 0.5–0.7 Å. The parameter β is related to the height of the molecule above the image plane of the metal surface. With a metal interlayer distance of Δ, then the image plane can be expected to be at about $\Delta/2$,[8,9] giving values of β around 1.6–2.0 Å for the different metals considered here. From these results we conclude that the vertical orientation is favored over a flat one within the pure electrostatic model considered here. According to the DFT results discussed in Sec. III B, however, the water molecule lies almost parallel against the surface. Thus the adsorption geometry is dictated by something other than the dipole-image interaction. We now move on to examine in detail the computed electronic structures of these adsorption systems obtained from our self-consistent first principles calculations.

D. Electron density and Mulliken analysis

Figure 5 displays electron density difference plots, obtained according to the procedure outlined in Sec. II, for the four water adsorption systems under consideration here. Such plots, which are consistent with those reported before for water monomer adsorption on close-packed metal surfaces,[18,25] provide an immediate overview for how the electrons rearrange upon adsorption. In particular, it can be seen that the major region of charge rearrangement is located along the water-metal bond axis. In the case of Ru, Rh, and

TABLE II. Valence Mulliken population analysis (in e) for adsorbed H_2O and the metal atom directly beneath it on each of the four metal surfaces. The values corresponding to free water and the metal atoms in the top layer of the clean metal surfaces are also provided.

		s	p	d	Total
Ru(0001)	H	0.61	0.00	0.00	0.61
	H	0.60	0.00	0.00	0.60
	O	1.85	4.91	0.00	6.76
	Ru	0.54	0.50	6.93	7.96
Rh(111)	H	0.60	0.00	0.00	0.60
	H	0.60	0.00	0.00	0.60
	O	1.86	4.92	0.00	6.78
	Rh	0.98	0.00	8.04	9.02
Pd(111)	H	0.61	0.00	0.00	0.61
	H	0.61	0.00	0.00	0.61
	O	1.85	4.93	0.00	6.78
	Pd	0.62	0.15	9.22	9.99
Ag(111)	H	0.57	0.00	0.00	0.57
	H	0.57	0.00	0.00	0.57
	O	1.86	4.99	0.00	6.86
	Ag	0.67	0.50	9.81	10.98
Free water	H	0.47	0.00	0.00	0.47
	H	0.47	0.00	0.00	0.47
	O	1.89	5.16	0.00	7.05
Clean surface	Ru	0.66	0.54	6.96	8.17
	Rh	1.05	0.00	8.08	9.13
	Pd	0.69	0.17	9.28	10.15
	Ag	0.78	0.49	9.82	11.09

Pd a clear d_{z2}-like depletion region is observed for the metal atom to which water is bonded, accompanied by a population of equatorial d-orbitals. Actually, this is consistent with the topology of the $W(\mathbf{r})$ function discussed in Sec. III A, which implies a reduction in Pauli repulsion that allows the H_2O molecule to approach closer to the metal surface. In addition a small electron gain domain is observed along the O-metal bond, whose magnitude increases when moving from right to left along the periodic series. In each case charge redistribution on the neighboring metal atoms is considerably smaller. Moreover, compared to the three other metals, the density rearrangement at the Ag surface is less pronounced.

A complimentary approach for extracting general information about the charge rearrangement in these systems is provided by a Mulliken population analysis (Table II).[49] This suggests that the overall charge transfer between the adsorbed water molecules and the substrate is very small. The total charge transfer from the adsorbed water molecule to the metal never exceeds $0.03e$. This is something that could already be inferred from the electron density difference plots displayed in Fig. 5. More significant, in terms of the Mulliken population analysis, is an internal charge rearrangement within the water molecule. Specifically we find that compared to the gas phase, in all four adsorption systems, an $\approx 0.2e$ internal charge transfer is observed from the O p-like orbitals to the two H s-like orbitals.

Moving now to the substrates, the Mulliken analysis indicates that the metal atom directly beneath the water molecule is slightly depopulated by $0.1-0.2e$ with a corresponding electron transfer into s- and d-like orbitals of neighboring surface atoms. In particular, the s, p, and d components are depleted by $\leq 0.1e$, $\leq 0.04e$, and $\leq 0.05e$, respectively. These electrons are gained uniformly by the other metal atoms in the topmost surface layer of the metal. This behavior is again consistent with the $\Delta\rho$ plots (Fig. 5), since the observed strong charge rearrangement involves essentially an internal reorganization of axial and equatorial d-orbitals with only a small build up in density on the neighboring metal atoms. Although charge transfer between metal axial d to s orbitals has been said to contribute to water-metal bonding in more open surfaces,[50] we do not observe a net population gain of s orbitals for the systems considered here. Nevertheless, some role of sp states in the bonding cannot be ruled out, as will be discussed below.

E. Density of state analysis

Having obtained some overview of how the electrons rearrange in these systems, we now look in more detail at the specific orbitals involved in the water-metal interaction. To this end we examine the partial density of states for water adsorbed on each of the four metals considered here. Specifically, in Fig. 6 the PDOS of the H_2O molecule and of the metal atom of the atop site to which it is bonded are displayed relative to E_F. In addition, in order to rationalize consistently the absolute shifts experienced by the various water states when interacting with the substrate, we have also computed the effective potential at the vacuum level (V_∞) (Ref. 51) for both isolated and adsorbed water (see Table III).

Now let us consider the various water states, starting with the low energy $2a_1$- and $1b_2$-like water MOs, which appear around 22 and 10 eV below E_F, respectively. These orbitals are far below the metal valence band of each metal and can thus be expected to interact weakly with the metal states. Nevertheless, the $2a_1$ and $1b_2$ states after adsorption on Ag (Ru, Rh, and Pd) shift down in energy 5.6 (5.9–6.0) eV and 5.6 (5.8–5.9) eV, respectively. A careful inspection of the density of the individual Kohn–Sham eigenstates associated with these levels reveals that no mixing or hybridization with the substrate states takes place. Thus these shifts are due to an intrinsic adsorbate level resonance with the broad metal continuum of states in agreement with the Newns–Anderson model for the case of weak coupling between states.[52] Similar large shifts have been reported previously for H_2 adsorption on metals.[53,54] Although a direct relationship between the metal work function (Φ) and the magnitude of this shift for a given adsorbate state is not clear, larger Φ values seem to induce larger shifts (see Table III).

In the case of the $3a_1$ and $1b_1$ states these undergo larger absolute shifts down in energy than those due to coupling with the metal continuum (Table III). This extra energy stabilization is a signature of covalent coupling between these water levels and the substrate. Indeed inspection of the density associated with the individual Kohn–Sham eigenstates within these peaks reveals mixing with substrate d states. We will say more about this mixing in Sec. III F when considering with which region(s) of the metal d-bands these orbitals interact. Notice that for the case of Ag an extra less promi-

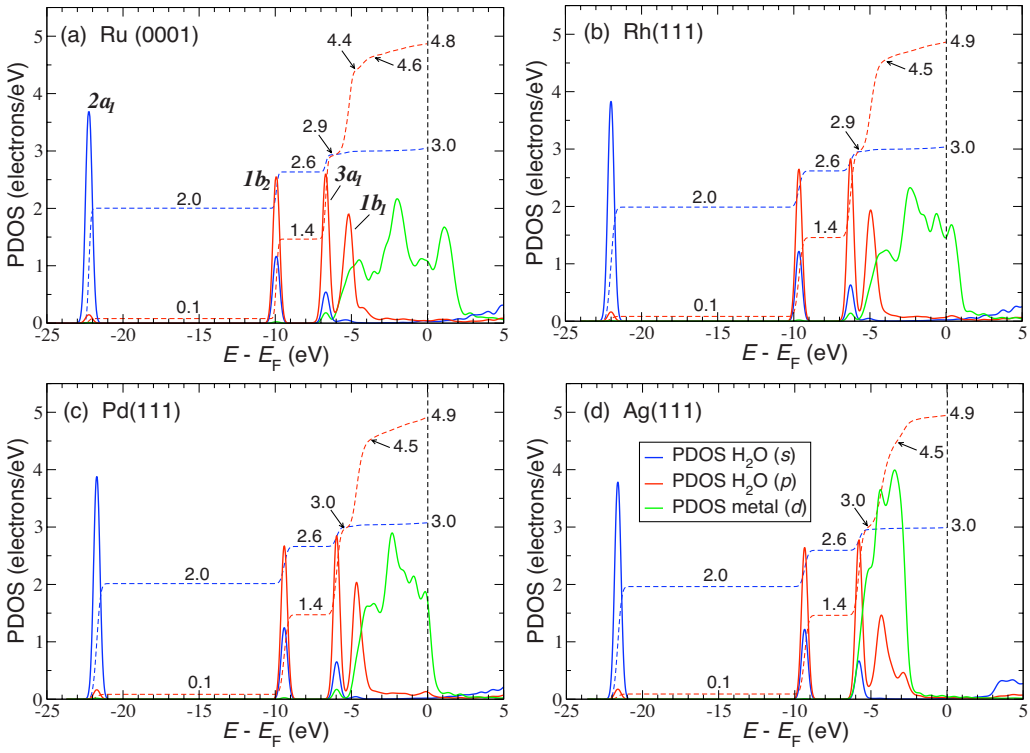

FIG. 6. (Color online) PDOS for water adsorbed on: (a) Ru(0001), (b) Rh(111), (c) Pd(111), and (d) Ag(111). The solid curves are the PDOS projected onto the *s* and *p* orbitals of the water molecule, and the *d* orbitals of the metal atom upon which H_2O is adsorbed. The dashed curves and the accompanying numbers correspond to *s*- and *p*-band integrations. The energy zero is the Fermi level.

nent peak at 3 eV below E_F is also observed [Fig. 6(d)]. For the current discussion only the second more intense peak below E_F has been taken into account.

In order to establish any possible contribution to the level shifts observed here from changes in the geometry of the water molecule upon adsorption, reference calculations involving gas phase water molecules but at the geometries assumed after adsorption on each surface, have also been performed. As shown in Table III, the effect of water geometry is pretty small, only in the case of the $2a_1$ orbital are slightly larger differences observed (<0.1 eV). Thus we rule out small structural variations in the adsorbed water molecules as being behind the trends in adsorption being discussed here.

In addition to energy, the broadening of a particular peak is another important characteristic that can provide insight into the nature of bonding.[55] The greater the overlap between individual orbitals involved in a given state, the greater the broadening. Taking an isolated water molecule as a reference,[56] the change in the width of the valence states upon adsorption is qualitatively consistent with the proposed bonding scheme described above: (i) The $2a_1$ and $1b_2$ peak widths remain nearly unperturbed; (ii) the $3a_1$ peak is slightly broadened (<0.1 eV); and (iii) the $1b_1$ peak undergoes a noticeable enlargement (0.3–0.5 eV), which depends on the considered metal. We note though that consistent with the weak bonding in these adsorption systems, the broadening, even for the $1b_1$, peak is not particularly large.

TABLE III. Computed work function (Φ), effective potential at the vacuum limit (V_∞) after water adsorption, and water level shifts—understood as shifts down in energy—with respect to a free water molecule at its equilibrium geometry or at the geometries observed after adsorption (values in parenthesis). Water level shift values are referred to the corresponding V_∞ of the given metal. All values are in eV.

	Ru(0001)	Rh(111)	Pd(111)	Ag(111)
Φ	4.75[a]	5.15[a]	5.38[a]	4.40[a]
V_∞	3.73	4.08	4.24	4.03
$2a_1$	−5.91 (−6.01)	−6.01 (−6.10)	−5.89 (−5.96)	−5.63 (−5.66)
$1b_2$	−5.82 (−5.83)	−5.87 (−5.93)	−5.78 (−5.81)	−5.57 (−5.60)
$3a_1$	−6.37 (−6.35)	−6.28 (−6.26)	−6.14 (−6.13)	−5.80 (−5.74)
$1b_1$	−6.93 (−6.88)	−7.00 (−6.96)	−6.85 (−6.82)	−6.35 (−6.32)

[a]Similar values have been reported before (Refs. 57 and 58).

F. Frontier orbital picture

Now we look in more detail at the partial densities of states for these systems. In particular, how the PDOS change upon adsorption. We then use this information and what we have learned already from Secs. III D and III E to construct frontier orbital diagrams for these adsorption systems.

As pointed out before, the major surface-adsorbate interactions involve the $3a_1$ and $1b_1$ orbitals of water. The initial metal orbitals that are able to overlap efficiently with these adsorbate orbitals can be inferred by inspecting the PDOS depletion regions with respect to the clean surface. The regions where states disappear indicate states that are involved in the bonding. Regions where new states are created—gain regions—denote the formation of new bonding and/or antibonding states. We use this information to restore the corresponding frontier orbital diagrams[38,59,60] within the context of a tight-binding model.[61] In particular, we have considered an orbital model perspective in the framework of Hoffmann's

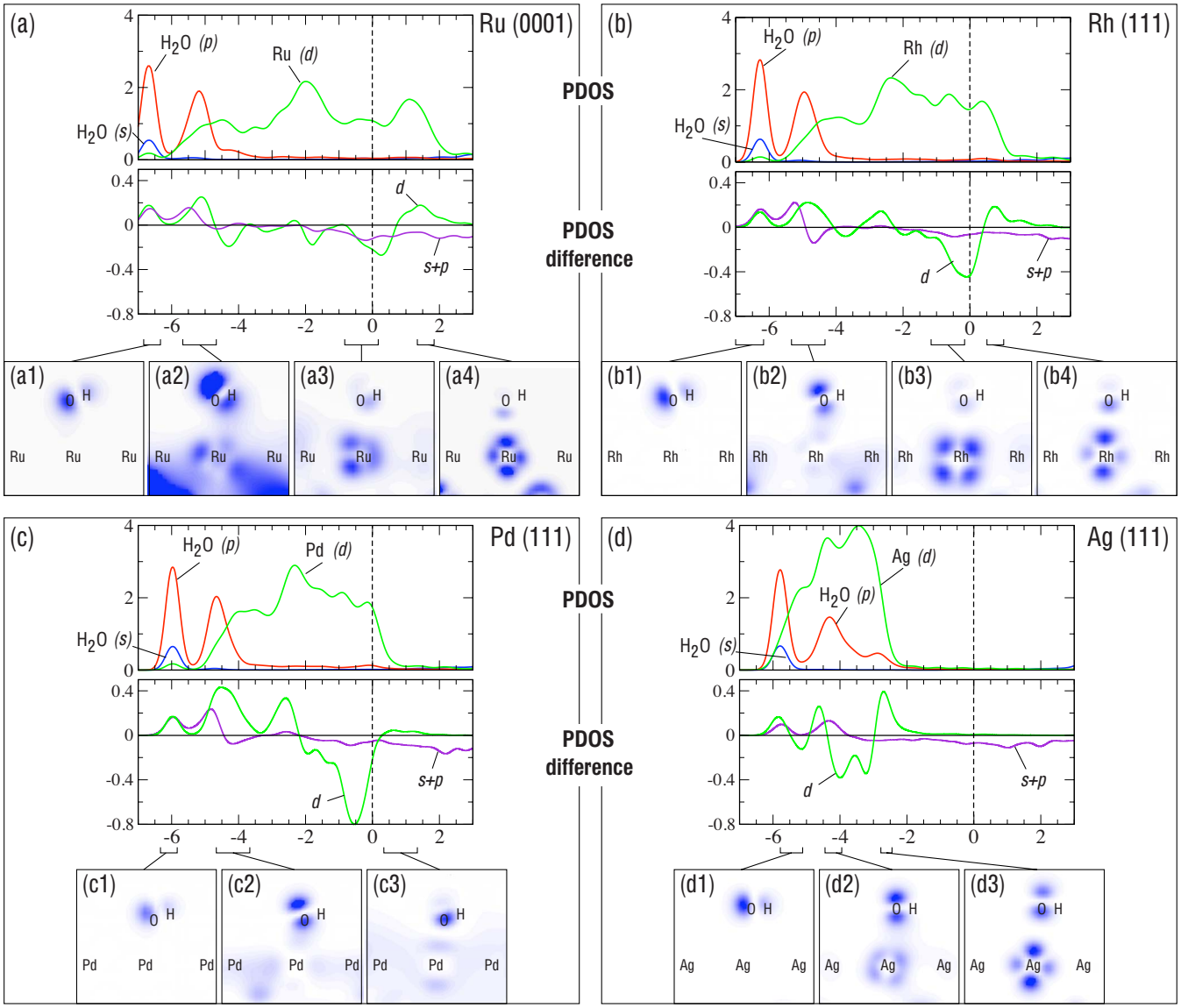

FIG. 7. (Color online) PDOS (same as Fig. 6) and PDOS difference plots projected onto $(s+p)$ and d states of the atop metal atom upon which the water is adsorbed. Negative (positive) values stand for depletion (creation) of metal states. The insets display electron density contour plots (along the P2 plane in Fig. 5) associated with individual Kohn–Sham eigenstates. The energy zero is E_F and, as with Fig. 6, the units of the y axes are electrons/eV.

interaction diagram concepts,[55,62–64] which have proven to be well suited to interpreting the nature of bonding in adsorption systems.

From inspection of the PDOS plots in Fig. 7 we find that the H_2O $3a_1$ (left most peak) interacts mainly with a narrow region of the d-band, leading to the formation of fully occupied bonding and antibonding states. Thus it turns out that the $3a_1$ interaction with the d-metal band is destabilizing. Mainly this is due to the fact that the $3a_1$ state is too far below E_F and, therefore, the resultant interaction is too weak to enable the antibonding states to rise above E_F and become depopulated. Indeed, the mixing of the d and $3a_1$ orbitals is quite small. The corresponding insets of Fig. 7 clearly show that the bonding states are almost exclusively of $3a_1$ character with very little d character apparent. The $3a_1$ orbital interacts more weakly as one moves to the left of the series, but essentially the nature and extent of this interaction is qualitatively the same for the four $4d$ metals. Therefore it will not be further considered.

As we have said, the H_2O $1b_1$ orbital is the closest one to the E_F of each metal and, therefore, able to interact most strongly with the states of the metal. This is seen by the prominent d depletion region around E_F for Ru, Rh, and Pd (Fig. 7), and to a smaller extent sp depletion. Indeed, it is because the $1b_1$ orbital is orthogonal to the C_{2v} symmetry plane of the molecule, that water prefers to adsorb flat (small angle α) on the surface in order to maximize the interaction of this orbital with the substrate. The d depletion region around E_F becomes larger when moving from Ru to Pd, behavior which can be explained by the fact that the Pd(111) surface is the most chemically "soft," followed by Rh(111) and Ru(0001), as indicated by the $W(\mathbf{r})$ analysis (Sec. III A). It does not mean that water interacts most strongly with Pd, but rather that Pd is able to depopulate more easily its frontier orbitals. We conclude from the electron density difference plots (Fig. 5) and inspection of individual Kohn–Sham eigenstates that this portion of the d-band is formed essentially by d_{z^2}-like orbitals which are pointed directly toward

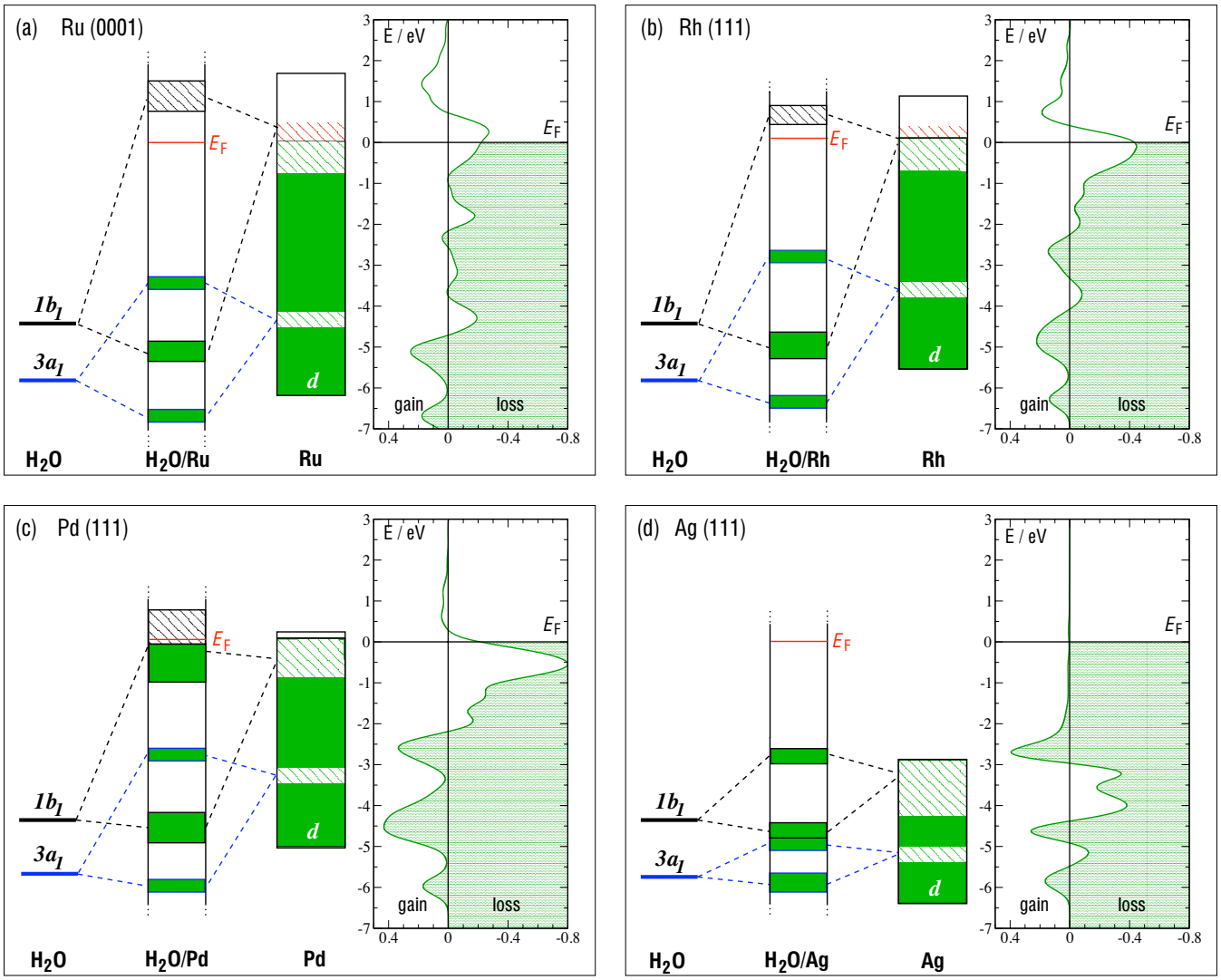

FIG. 8. (Color online) Schematic molecular level interaction diagrams for water monomer adsorption on (a) Ru(0001), (b) Rh(111), (c) Pd(111), and (d) Ag(111). The principal interactions between the $1b_1$ and d states of the substrate are indicated. Solid (dashed) filled bars indicate occupied (empty) states. For each case, the graphs on the right are d projected PDOS difference plots (same as those in Fig. 7).

the H_2O $1b_1$ orbital, enhancing effective overlap. To a lesser extent the H_2O $1b_1$ orbital also interacts with deeper d states as indicated by the additional depletion regions just below the main depletion domain (Fig. 7).[65] Such interactions result in the formation of new bonding and antibonding states between the d-band and the $1b_1$ orbitals. Especially for the cases of Ru and Rh, the corresponding MOs associated with the antibonding d_{z2}-$1b_1$ states clearly show a d_{z2} and $1b_1$ mixture with the presence of a nodal plane [Fig. 7, insets (a4) and (b4)]; antibonding states without d_{z2} character have been detected just below E_F as well [Fig. 7, insets (a3) and (b3)]. Since the d orbitals involved in the bonding are initially located very close to E_F it implies that the antibonding states appear above the E_F. The case of Ag is a different story, since E_F is $\approx$2 eV above the top of the d-band. It means that the antibonding states will be fully occupied and no covalent stabilization can take place. The small adsorption energy computed for water on Ag(111), -0.15 eV (Table I), is, therefore, due to electrostatic interactions. Since water adsorbs flat on Ag, and the pure metal image dipole interaction favors a vertical orientation (Sec. III B), we speculate that quadrupole-quadrupole[66] interactions might be responsible for the observed adsorption geometry of water on Ag(111).

Bringing together all the points discussed so far, we arrive at the schematic set of frontier orbital diagrams sketched in Fig. 8, which provide a general overview of the main interactions dictating the bonding in these systems. We focus now on the specific differences along the investigated 4d series. As one goes from Ru to Pd the d orbitals at the top of d-band are more populated and the d density changes consequently become larger. Moreover, the center of gravity of the d-band falls. In the case of Ag, the fully occupied antibonding MO derived from the interaction of H_2O $1b_1$ and the top of the d-band lies below E_F. Thus this is a repulsive two-center four-electron interaction. The situation is different for the cases of Ru, Rh, and Pd, where the antibonding component of the interaction with the most energetic d metal states rises totally (Ru and Rh) or partially (Pd) above E_F [Figs. 8(a)–8(c)]. In these cases the electrons associated with such antibonding levels can be dumped at the E_F contributing to a stabilization of the system.[55] This stabilization mechanism becomes less effective when moving from Ru to Pd, since

the antibonding states get progressively occupied. Moreover, if one compares the corresponding frontier orbital diagrams, it can be observed that the energy gain produced by the orbital mixing—energy difference between H_2O $1b_1$ level and the corresponding new bonding state formed—decreases when moving right along the series. These two facts together justify the adsorption energy trends discussed in Sec. III B, i.e., the less the stabilization is, the less the adsorption energy is.

It is noteworthy that according to the PDOS difference plots the role of the *s* and *p* electrons in these adsorption systems is not negligible. As discussed in Sec. III E the reported *sp* to *d* charge transfer is not picked up by the Mulliken analysis. Nevertheless, a depopulation of *s* and *p* states along a broad region around E_F denotes the participation of these states in the water-metal bonding. Compared with *d* states, their role is less prominent, but not negligible. In particular, the interaction of water with such states could be behind the origin of the small electron gain region along the water-metal axis (Fig. 5), corresponding to the new states formed at low energies (around the H_2O $3a_1$ and $1b_1$), as suggested by Li *et al.*[50] Indeed, this fact implies that likely some sort of a d_{z2}-*sp* hybrid type orbitals are those that interact with H_2O $3a_1$ and $1b_1$ orbitals.

IV. DISCUSSION AND CONCLUSIONS

The adsorption of H_2O monomers on 4*d* metal surfaces has been investigated through a systematic DFT study. The aim has been to extract insight in to the general features that govern the bonding in such adsorption systems. Let us now briefly summarize the key conclusions and discuss the main results of this paper in a somewhat broader context:

(i) The interaction between the H_2O $1b_1$ orbital and the top of the metal *d*-band results in the formation of a set of bonding and antibonding states. The ability of the metal to stabilize this two-center four-electron interaction by depopulating the antibonding states controls the trends observed in the water adsorption energies. When the metal *d*-band is partially occupied, these states appear above E_F and the mentioned depopulation can take place. This stabilization mechanism is viable for Ru and Rh, less favorable for Pd and unfeasible for Ag. Clearly this is an interpretation of the bonding in the language of covalency. This interpretation is largely equivalent with an alternative interpretation of the bonding in these systems, where similar $\Delta\rho$ plots to those shown in Fig. 5 have been interpreted in terms of enhancement of the overlap between orbitals as a consequence of a reduction in Pauli repulsion between the $1b_1$ orbital and axial metal *d* orbitals,[25,31] resulting in a closer approach of the water molecule to the metal surface.

(ii) Atop sites are preferred since this allows for the best soft-soft interactions in terms of the reactivity index, $W(\mathbf{r})$, which controls the final molecular orientation as well.

(iii) Adsorption at atop sites and a flat water orientation is the preferred mode of adsorption for water on these and most likely several other close-packed late transition metal surfaces. Both DFT (Refs. 6 and 18–20) and many indications from experiment[10–17] consistently agree that such a structural model is correct. Of course, we are not suggesting that water will adsorb like this on every metal surface. Indeed, the realization that the $1b_1$ water MO is key to many of the properties of water on metals together with the soft-soft interaction concept analyzed in terms of the reactivity function, $W(\mathbf{r})$, provides a useful tool to predict other adsorption configurations on as-yet not studied surfaces.

Finally, although it was beyond the scope of the present study, to arrive at a complete understanding of how water molecules bond to metal surfaces it will, of course, be interesting and important to understand the role van der Waals dispersion forces play. With the emergence of various DFT-based schemes to account for such interactions[67–74] and quantum Monte Carlo, it seems that an answer to this question is not too far away.

ACKNOWLEDGMENTS

J. C. acknowledges financial support from the Alexander von Humboldt Foundation and the Royal Society. A. M's work was supported by a EURYI award (see www.esf.org/euryi) and the EPSRC.

[1] P. A. Thiel and T. E. Madey, Surf. Sci. Rep. **7**, 211 (1987).
[2] M. A. Henderson, Surf. Sci. Rep. **46**, 1 (2002).
[3] A. Verdaguer, G. M. Sacha, H. Bluhm, and M. Salmeron, Chem. Rev. **106**, 1478 (2006).
[4] A. Hodgson and S. Haq, Surf. Sci. Rep. (unpublished).
[5] A. Michaelides, V. A. Ranea, P. L. de Andres, and D. A. King, Phys. Rev. Lett. **90**, 216102 (2003).
[6] V. A. Ranea, A. Michaelides, R. Ramirez, J. A. Verges, P. L. de Andres, and D. A. King, Phys. Rev. B **69**, 205411 (2004).
[7] J. Mahanty and N. H. March, J. Phys. C **9**, 2905 (1976).
[8] B. L. Maschhoff and J. P. Cowin, J. Chem. Phys. **101**, 8138 (1994).
[9] E. V. Chulkov, V. M. Silkin, and P. M. Echenique, Surf. Sci. **437**, 330 (1999).
[10] S. Andersson, C. Nyberg, and C. G. Tengstal, Chem. Phys. Lett. **104**, 305 (1984).
[11] B. W. Callen, K. Griffiths, and P. R. Norton, Phys. Rev. Lett. **66**, 1634 (1991).
[12] N. Pangher, A. Schmalz, and J. Haase, Chem. Phys. Lett. **221**, 189 (1994).
[13] M. Nakamura and M. Ito, Chem. Phys. Lett. **325**, 293 (2000).
[14] T. Mitsui, M. K. Rose, E. Fomin, D. F. Ogletree, and M. Salmeron, Science **297**, 1850 (2002).
[15] C. G. Sánchez, Surf. Sci. **527**, 1 (2003).
[16] K. Morgenstern and K.-H. Rieder, J. Chem. Phys. **116**, 5746 (2002).
[17] K. Morgenstern and K.-H. Rieder, Chem. Phys. Lett. **358**, 250 (2002).
[18] S. Meng, E. G. Wang, and S. Gao, Phys. Rev. B **69**, 195404 (2004).
[19] D. Sebastiani and L. Delle Site, J. Chem. Theory Comput. **1**, 78 (2005).
[20] P. Vassilev, R. A. van Santen, and M. T. M. Koper, J. Chem. Phys. **122**, 054701 (2005).
[21] J. Knudsen, A. U. Nilekar, R. T. Vang, J. Schnadt, E. L. Kunkes, J. A. Dumesic, M. Mavrikakis, and F. Besenbacher, J. Am. Chem. Soc. **129**, 6485 (2007).
[22] A. Michaelides, Appl. Phys. A: Mater. Sci. Process. **85**, 415 (2006).
[23] A. Michaelides, Faraday Discuss. **136**, 287 (2007).
[24] A. Michaelides, A. Alavi, and D. A. King, J. Am. Chem. Soc. **125**, 2746 (2003).
[25] H. Ogasawara, B. Brena, D. Nordlund, M. Nyberg, A. Pelmenschikov, L. G. M. Pettersson, and A. Nilsson, Phys. Rev. Lett. **89**, 276102 (2002).
[26] A. B. Anderson, Surf. Sci. **105**, 159 (1981).

[27] E. Spohr and K. Heinzinger, Chem. Phys. Lett. **123**, 218 (1986).
[28] H. Yang and J. L. Whitten, Surf. Sci. **223**, 131 (1989).
[29] S. Meng, L. F. Xu, E. G. Wang, and S. Gao, Phys. Rev. Lett. **89**, 176104 (2002).
[30] A. Michaelides and P. Hu, J. Am. Chem. Soc. **123**, 4235 (2001).
[31] M. Cavalleri, H. Ogasawara, L. G. M. Pettersson, and A. Nilsson, Chem. Phys. Lett. **364**, 363 (2002).
[32] M. D. Segall, P. J. D. Lindan, M. J. Probert, C. J. Pickard, P. J. Hasnip, S. J. Clark, and M. C. Payne, J. Phys.: Condens. Matter **14**, 2717 (2002).
[33] D. Vanderbilt, Phys. Rev. B **41**, 7892 (1990).
[34] J. P. Perdew, K. Burke, M. Ernzerhof, Phys. Rev. Lett. **77**, 3865 (1996); J. P. Perdew, K. Burke, M. Ernzerhof, *ibid.* **78**, 1396 (1997).
[35] H. J. Monkhorst and J. D. Pack, Phys. Rev. B **13**, 5188 (1976).
[36] The computed values (a_{Ru}=2.720 Å; c_{Ru}=4.284 Å; a_{Rh}=3.893 Å; a_{Pd}=3.930 Å; a_{Ag}=4.139 Å) are in good agreement with those computed using an all-electron FP-LAPW method (Refs. 75 and 76) and are overestimated by less than 2.5% with respect to experimental data [from J. Heyd *et al.* (Ref. 77)].
[37] Computed here as **k**-averaged states for a given energy interval.
[38] K. Fukui, Science **218**, 747 (1982).
[39] K. Fukui, T. Yonezawa, and H. Shingu, J. Chem. Phys. **20**, 722 (1952).
[40] S. Wilke, M. H. Cohen, and M. Scheffler, Phys. Rev. Lett. **77**, 1560 (1996).
[41] R. G. Pearson, J. Am. Chem. Soc. **85**, 3533 (1963).
[42] R. G. Pearson, Science **151**, 172 (1966).
[43] R. G. Parr and R. G. Pearson, J. Am. Chem. Soc. **105**, 7512 (1983).
[44] J. L. F. Da Silva, C. Stampfl, and M. Scheffler, Phys. Rev. B **72**, 075424 (2005).
[45] It is worth mentioning that similar $W(\mathbf{r})$ plots to that reported here for Pd(111) has been found also by other authors (Ref. 44).
[46] Computed here as the total energy of the water-metal system minus the energy of an isolated water molecule minus the energy of the clean metal slab. The isolated water molecule is computed in a 15 Å cube.
[47] A. Nilsson and L. G. M. Pettersson, Surf. Sci. Rep. **55**, 49 (2004).
[48] Considering q values in the range $\pm 0.76e$ to $\pm 0.86e$ has a minor effect on the computed U_{se} differences, typically less than 3 meV with respect to the values plotted in Fig. 4 for $q=\pm 0.80e$.
[49] The Mulliken population analysis, which is, of course, a rather arbitrary method for charge partitioning, is performed by projecting the plane wave states onto a localized basis set by the projection technique of Sanchez-Portal *et al.* (Ref. 78).
[50] J. Li, S. Zhu, Y. Li, and F. Wang, Phys. Rev. B **76**, 235433 (2007).
[51] The effective potential has been separated here into two different terms, electrostatic and exchange-correlation potentials. Whilst the former converges relatively quickly within the vacuum, the later has a longer decay length. Therefore, since the exchange-correlation potential converges to zero in the vacuum gap, we have only considered the electrostatic potential to compute V_∞.
[52] D. M. Newns, Phys. Rev. **178**, 1123 (1969).
[53] B. Hammer and J. K. Nørskov, Surf. Sci. **343**, 211 (1995).
[54] B. Hammer and M. Scheffler, Phys. Rev. Lett. **74**, 3487 (1995).
[55] R. Hoffmann, Rev. Mod. Phys. **60**, 601 (1988).
[56] Measured at the half-height of the band and considering the same smearing for all cases, including the discrete states of the gas phase H_2O.
[57] A. Migani and F. Illas, J. Phys. Chem. B **110**, 11894 (2006).
[58] M.-L. Bocquet, A. M. Rappe, and H.-L. Dai, Mol. Phys. **103**, 883 (2005).
[59] W. L. Jorgensen and L. Salem, *The Organic Chemist's Book of Orbitals* (Academic, New York, 1973).
[60] J.-Y. Saillard and R. Hoffmann, J. Am. Chem. Soc. **106**, 2006 (1984).
[61] F. M. Mueller, Phys. Rev. **153**, 659 (1967).
[62] S.-S. Sung and R. Hoffmann, J. Am. Chem. Soc. **107**, 578 (1985).
[63] G. Papoian, J. K. Nørskov, and R. Hoffmann, J. Am. Chem. Soc. **122**, 4129 (2000).
[64] W. V. Glassey and R. Hoffmann, J. Phys. Chem. B **105**, 3245 (2001).
[65] Up to perhaps three partially overlapping interaction regions can be identified in the *d*-band of each metal, especially for the case of Ru and less so as the *d*-band narrows upon moving right in the periodic series.
[66] A. J. Stone, *The Theory of Intermolecular Forces, International Series of Monographs on Chemistry* (Oxford University Press, Oxford, England, 1996).
[67] B. Santra, A. Michaelides, M. Fuchs, A. Tkatchenko, C. Filippi, and M. Scheffler, J. Chem. Phys. **129**, 194111 (2008).
[68] Q. Wu and W. Yang, J. Chem. Phys. **116**, 515 (2002).
[69] S. Grimme, J. Comput. Chem. **25**, 1463 (2004).
[70] P. Jurečka, J. Čverny, P. Hobza, and D. R. Salahub, J. Comput. Chem. **28**, 555 (2007).
[71] M. Dion, H. Rydberg, E. Schröder, D. C. Langreth, and B. I. Lundqvist, Phys. Rev. Lett. **92**, 246401 (2004).
[72] A. D. Becke and E. R. Johnson, J. Chem. Phys. **122**, 154104 (2005).
[73] P. L. Silvestrelli, Phys. Rev. Lett. **100**, 053002 (2008).
[74] O. A. von Lilienfeld, I. Tavernelli, U. Rothlisberger, and D. Sebastiani, Phys. Rev. Lett. **93**, 153004 (2004).
[75] J. L. F. Da Silva, C. Stampfl, and M. Scheffler, Surf. Sci. **600**, 703 (2006).
[76] J. Paier, M. Marsman, K. Hummer, G. Kresse, I. C. Gerber, and J. G. Ángyán, J. Chem. Phys. **124**, 154709 (2006).
[77] J. Heyd and G. E. Scuseria, J. Chem. Phys. **121**, 1187 (2004).
[78] D. Sanchez-Portal, E. Artacho, and J. M. Soler, Solid State Commun. **95**, 685 (1995).